THE JOURNAL OF PHYSICAL CHEMISTRY A

Article

Photophysical and Electrochemical Properties of Thienylnaphthalimide Dyes with Excellent Photostability

Takatoshi Inari, Minori Yamano, Ayaka Hirano, Kosuke Sugawa, and Joe Otsuki

J. Phys. Chem. A, **Just Accepted Manuscript** • DOI: 10.1021/jp502535n • Publication Date (Web): 24 Jun 2014

Photophysical and Electrochemical Properties of Thienylnaphthalimide Dyes with Excellent Photostability

*Takatoshi Inari, Minori Yamano, Ayaka Hirano, Kosuke Sugawa, and Joe Otsuki**

College of Science and Technology, Nihon University, 1-8-14 Kanda Surugadai, Chiyoda, Tokyo 101-8308, Japan

S Supporting Information

ABSTRACT: The development of robust dyes is a highly important theme for any applications of dyes. Here we present photophysical and electrochemical characterization of a set of robust dyes based on thienylnaphthalimide unit. The set comprises of the thienylnaphthalimide derivatives with phenyl- (Ph-), 4-nitrophenyl- (NO_2Ph-), and 4-(diphenylamino)phenyl (Ph_2NPh-) substituents as exemplars covering electron-withdrawing to electron donating groups. The fluorescence quantum yields of the Ph-TNI increases as the solvent polarity increases, while that of Ph_2NPh-TNI showed the opposite trend. Changes in the rates of nonradiative decay were found to be a major factor for these contrasting behaviors. Cyclic voltammetry showed that the substituent effects were more apparent for the HOMO energies rather than the LUMO energies. Density functional theory calculations showed that the first singlet excited state of these

compounds is a $^1\pi,\pi^*$ state with a significant charge transfer character. Ph-TNI and Ph_2NPh-TNI are much more stable against photodegradation than coumarin and fluorescein dyes.

Keywords: Absorption, Excited State, Fluorescence, Fluorophore, Push-pull

INTRODUCTION

Organic fluorescent dyes are used for a wide range of applications including lasers,[1] sensors,[2-4] and solar cells,[5-6] and so on. Rylene dyes have attracted attention since they possess prominent chemical, thermal, and photo stability.[7] Rylenes are based on naphthalene units linked in the peri positions. They are often used in the forms of di- or tetra-carboxylic acids and their derivatives.[7-9] 1,8-naphthalic acid is the simplest member of the rylene dicarboxylic acid series.[6, 10] Fluorescent dyes based on 1,8-naphthalic acid may have the following advantages. (i) The parent structure is simple enough, which makes it possible to synthesize a wide variety of derivatives with minimum cost. (ii) It can be assumed that they are less prone to π-π aggregation compared to larger rylene derivatives. (iii) The dicarboxylic acid group can be used to tag the fluorophore through the formation of the imide bond to another functional fragment such as a unit for molecular recognition. Indeed, 1,8-naphthalimide (NI) based chromophores have been developed for various applications including DNA-oxidizing agents,[11-12] pH indicators,[13-14] sensors for various cationic and anionic species,[15-27] and emitters for organic light-emitting diodes.[28] As the π-system of NI is relatively small, it only absorbs at ~340 nm in the UV region,[29] although substitution by an amino group at the 4-position brings the absorption up to ~420 nm. It is desirable to bring the absorption further to the red so that visible light can be used to excite the dye and autofluorescence or background fluorescence can be avoided in the case of biological

and materials applications. It is also desirable to develop a multiple-color set of dyes to enable multicolored experiments as well as Förster-type resonance energy transfer experiments.

Thus we set out to prepare longer-wavelength absorbing dyes on the basis of NI core. To make the compound to absorb light in a longer wavelength region, we decided to extend the π-conjugation of the NI core with a thiophene unit rather than with use of perylene-3,4-dicarboximide. Potential advantages of this choice includes a higher solubility or less aggregation tendency, and more facile synthesis of 4-thienyl-1,8-naphthalimide and its derivatives than perylene-3,4-dicarboximide and its derivatives. Thiophene and oligothiophenes are chemically stable and have attracted attention as functional π-systems for optoelectronic applications.[10, 30] Despite the desirable properties of thiophene, only a few investigations have been reported for thienylnaphthalimide systems.[31-34] Our basic design for the dyes in this study is presented in Figure 1, in which a set of "tuning" groups were introduced into the parent thienylnaphthalimide structure. For the tuning, phenyl (Ph-TNI), 4-nitrophenyl (NO_2Ph-TNI), and 4-(diphenylamino)phenyl (Ph_2NPh-TNI) groups were introduced, which covers from electron-withdrawing to electron-donating groups. Here we report the preparation, photophysical and redox properties, and photostability of these new dyes. While photophysical properties including solvent effects were extensively investigated for the parent NI and its derivatives, in which substituents are directly introduced onto the naphthalene core,[35-42] neither detailed photophysics nor solvent effects have been reported for π-extended naphthalimide chromophores as far as we are aware of.

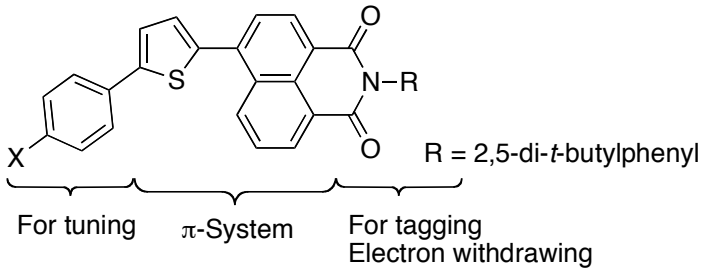

Ph-TNI: X- = H-
NO_2Ph-TNI: X- = O_2N-
Ph_2NPh-TNI: X- = Ph_2N-

Figure 1. Thienylnaphthalimide dyes.

EXPERIMENTAL SECTION

Synthesis in General. Dehydrated tetrahydrofuran was purchased from Kanto Chemical. Flash column chromatography was carried out using Kanto Chemical Silica Gel 60. Gel permeation chromatography was performed using a Japan Analytical Industry LC-9201 system equipped with columns, Jaigel-1H and Jaigel-2H. The retention volume V_R is given for each compound. ^{1}H and ^{13}C NMR spectra were measured on a JEOL JNM-ECX400 spectrometer (400 MHz for ^{1}H and 100 MHz for ^{13}C). Atmospheric pressure chemical ionization (APCI) high-resolution mass spectrometry (HRMS) were conducted on an Agilent LC/MCD TOF 1100 spectrometer. The dyes were prepared according to Scheme 1. *N*-(2,5-di-*t*-butylphenyl)-4-bromo-1,8-napththalimide was prepared from commercial 4-bromo-1,8-naphthalic anhydride according to a literature procedure.[43] All the reactions for the final steps described below were carried out in air.

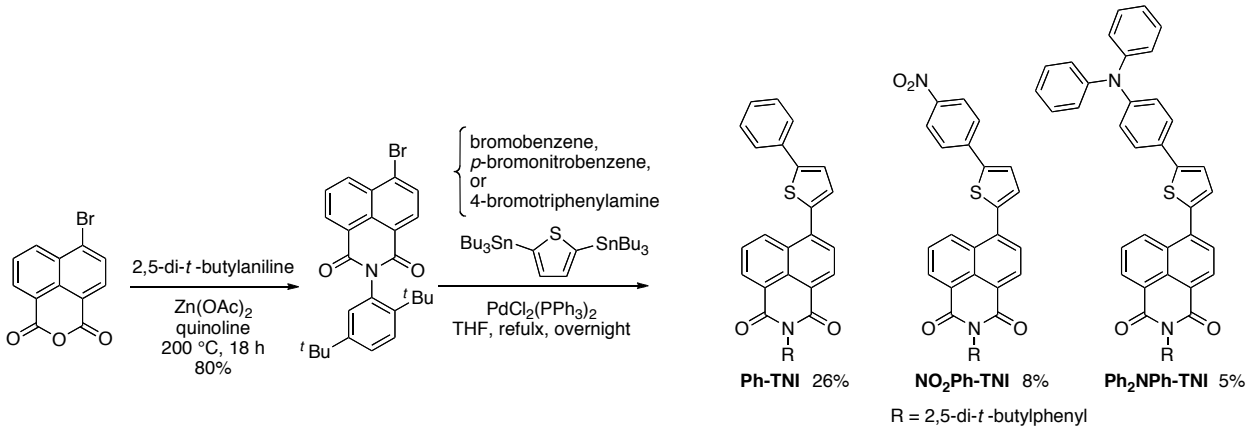

Scheme 1. Preparation of thienylnaphthalimides.

Ph-TNI. A mixture of *N*-(2,5-di-*t*-butylphenyl)-4-bromo-1,8-napththalimide (500 mg, 1.08 mmol), bromobenzene (345 mg, 1.15 mmol), 2,5-bis(tributylstannyl)thiophene (728 mg, 1.10 mmol), and dichlorobis(triphenylphosphine)palladium(II) (70 mg, 0.10 mmol) in tetrahydrofuran (120 mL) was refluxed overnight. The solvent was evaporated, leaving a residue, which was purified through column chromatography (SiO_2, hexane/chloroform = 1/1) and GPC to afford a yellow solid (132 mg, 0.285 mmol, 26%).

TLC (SiO_2, $CHCl_3$): R_f = 0.51. GPC: V_R = 179 mL. ^{1}H NMR ($CDCl_3$): δ (ppm) = 1.30 (9H, s), 1.33 (9H, s), 7.01 (1H, d, J = 2.4 Hz), 7.33–7.40 (2H, m), 7.42–7.45 (4H, m), 7.59 (1H, d, J = 7.3 Hz), 7.71 (2H, m), 7.83 (1H, t, J = 8.7 Hz), 7.91 (1H, d, J = 7.8 Hz), 8.67 (1H, d, J = 7.8 Hz), 8.71 (1H, d, J = 8.7 Hz), 8.81 (1H, d, J = 8.7 Hz). ^{13}C NMR ($CDCl_3$): δ (ppm) = 165.3, 165.0, 150.1, 147.0, 143.9, 139.3, 139.1, 133.8, 132.9, 132.7, 131.9, 131.3, 130.14, 130.08, 129.4, 129.2, 128.8, 128.5, 128.3, 127.8, 127.4, 126.3, 126.0, 124.0, 123.5, 122.3, 35.6, 34.3, 31.8, 31.3. APCI–HRMS ($CHCl_3$): m/z calculated for $C_{36}H_{34}NO_2S$ ($[MH]^+$), 544.2310; found, 544.2339. Analysis: calcd for $C_{36}H_{33}NO_2S$, C 79.52, H 6.12, N 2.58%; found, C 79.51, H 6.26, N 2.60%.

NO_2Ph-TNI. A mixture of *N*-(2,5-di-*t*-butylphenyl)-4-bromo-1,8-naphthalimide (354 mg, 0.752 mmol), 2,5-bis(tributylstannyl)thiophene (500 mg, 0.762 mmol), *p*-bromonitrobenzene (152 mg, 0.752 mmol), and dichlorobis(triphenylphosphine)palladium(II) (49 mg, 0.077 mmol) in tetrahydrofuran (120 mL) was refluxed overnight. The solvent was evaporated, leaving a residue, which was purified through column chromatography (SiO_2, hexane/chloroform = 1/1) and GPC to afford a yellow solid (33 mg, 0.057 mmol, 7.5%).

TLC (SiO_2, $CHCl_3$): R_f = 0.46. GPC: V_R = 179 mL. ^{1}H NMR ($CDCl_3$): δ (ppm) = 1.30 (9H, s), 1.33 (9H, s), 7.01 (1H, d, J = 2.3 Hz), 7.42–7.50 (2H, m), 7.60 (1H, d, J = 8.7 Hz), 7.63 (1H, d, J = 4.1 Hz), 7.80–7.89 (3H, m), 7.92 (1H, d, J = 7.8 Hz), 8.31 (2H, d, J = 8.7 Hz), 8.69 (1H, d, J = 7.3 Hz), 8.73 (2H, d, J = 8.2 Hz). ^{13}C NMR ($CDCl_3$): δ (ppm) = 165.2, 164.9, 150.2, 147.1, 143.9, 143.7, 142.0, 139.9, 138.4, 132.9, 132.3, 132.1, 131.2, 130.5, 130.1, 129.4, 128.9, 128.8, 127.8, 127.7, 126.5, 126.4, 126.2, 124.7, 123.6, 122.9, 35.6, 34.3, 31.8, 31.3. APCI–HRMS ($CHCl_3$): *m*/*z* calcd for $C_{36}H_{33}N_2O_4S$ ([MH]$^+$), 589.2161; found, 589.2136.

Ph_2NPh-TNI. A mixture of *N*-(2,5-di-*t*-butylphenyl)-4-bromo-1,8-naphthalimide (348 mg, 0.750 mmol), 4-bromotriphenylamine (249 mg, 0.768 mmol), 2,5-bis(tributylstannyl)thiophene (500 mg, 0.755 mmol), and dichlorobis(triphenylphosphine)palladium(II) (48 mg, 0.077 mmol) in tetrahydrofuran (120 mL) was refluxed overnight. The solvent was evaporated, leaving a residue, which was purified through column chromatography (SiO_2, hexane/chloroform = 1/1) and GPC to afford a red solid (23 mg, 0.032 mmol, 4.3%).

TLC (SiO_2, $CHCl_3$): R_f = 0.56. GPC: V_R = 171 mL. ^{1}H NMR ($CDCl_3$): δ (ppm) = 1.30 (9H, s), 1.33 (9H, s), 7.01 (1H, d, J = 2.3 Hz), 7.04–7.19 (8H, m), 7.26-7.33 (4H, m), 7.34–7.40 (2H, m), 7.45 (1H, dd, J = 8.7, 2.3 Hz), 7.51–7.62 (3H, m), 7.82 (1H, t, J = 8.2 Hz), 7.90 (1H, d, J = 7.8 Hz), 8.66 (1H, d, J = 7.8 Hz), 8.71 (1H, d, J = 7.3 Hz), 8.81 (1H, d, J = 8.7 Hz). ^{13}C NMR

($CDCl_3$): δ (ppm) = 165.3, 165.0, 150.1, 148.0, 147.4, 147.1, 143.9, 139.5, 138.1, 133.0, 132.7, 131.9, 131.3, 130.2, 130.1, 129.5, 128.8, 128.4, 127.8, 127.5, 127.3, 126.8, 126.3, 124.9, 123.5, 123.4, 123.1, 122.1, 35.6, 34.3, 31.8, 31.3. APCI–HRMS ($CHCl_3$): *m*/*z* calcd for $C_{48}H_{43}N_2O_4S$ ($[MH]^+$), 711.3045; found, 711.3104.

Physical Measurements and Computation. Absorption spectra were measured on a Shimadzu UV-2400 spectrometer. The molar absorption coefficients were obtained from the absorbance of 10 μM solutions prepared by weighing about 1 mg with a Mettler-Toledo UMX2 ultra-micro balance, whose readability is 0.1 μg. Fluorescence spectra were taken on a Jasco FP-8600 spectrometer. The spectrum of the excitation source was corrected using a SIC-844 standard detector and the wavelength-dependent sensitivity of the detector was corrected using a ESC-842 standard halogen lamp. Thus, the ordinate of the fluorescence spectra represents the relative number of photons per unit wavelength interval. Fluorescence quantum yields ϕ_{sample} were obtained by comparing the fluorescence spectra of the samples with that of rhodamine 6G ($\phi_{\text{ref}} = 0.94$ in ethanol[44]) using eq 1,[45]

$$\phi_{\text{sample}} = \phi_{\text{ref}} \frac{I_{\text{sample}}}{I_{\text{ref}}} \frac{1-10^{-A_{\text{ref}}}}{1-10^{-A_{\text{sample}}}} \frac{n_{\text{sample}}^2}{n_{\text{ref}}^2} \tag{1}$$

where I is the integrated fluorescence spectrum which is proportional to the number of emitted photons, A is the absorbance at the excitation wavelength, and n is the refractive index of the solvent. The subscript 'sample' means the compound of interest and 'ref' means the reference compound, which is rhodamine 6G in the present case. Hereafter, the subscript 'sample' is replaced by 'f', which stands for fluorescence. Fluorescence lifetimes were measured on a Hamamatsu Photonics Quantaurus-Tau C11367 system. The samples were excited with a light-

emitting diode at 405 nm and the fluorescence decay was monitored at λ_{max} (full width at half maximum: ca. 10 nm). Spectroscopic grade toluene, dimethylsulfoxide (DMSO), methanol (MeOH), 1,4-dioxane, and acetonitrile (MeCN) were purchased from Kanto Chemical and used as received. All photophysical measurements were performed using air-equilibrated solvents. Quantum yield and lifetime measurements were repeated for at least three separately prepared sample solutions. The error ranges and error bars represent the confidence interval of 68.3% obtained from Student's *t*-distribution.

Cyclic voltammetry was measured using a Hokuto Denko HZ-3000 electrochemical analyzer. A 1 mM sample solution in MeCN containing 0.1 M tetrabutylammonium hexafluorophosphate ($N(Bu)_4PF_6$) was purged with N_2. Pt electrodes were used as the working and counter electrodes. A Ag electrode was used as the quasi-reference electrode. The scan rate was 100 mV s^{-1}. The potential were referenced to the internal ferrocene/ferricenium couple added after each measurement. Anhydrous MeCN for the electrochemistry was purchased from Kanto Chemical. For the photostability evaluation, an Asahi Spectra LAX-Cute Xe-lamp (100 W, 400–700 nm) was used as the light source. Density functional theory (DFT) calculations were performed with Gaussian 09M[46] and GaussView run on a personal computer. The functional and basis set as well as options used are indicated in the relevant places in the Results and Discussion section.

RESULTS AND DISCUSSION

Synthesis. The three compounds were synthesized as shown in Scheme 1. The mixed Stille coupling of *N*-(2,5-di-*t*-butylphenyl)-4-bromo-1,8-naphthalimide, 2,5-bis(tributylstannyl)thiophene, and one of bromobenzene, *p*-bromonitrobenene, and 4-bromotriphenylamine followed by purification with silica gel column chromatography and gel

permeation chromatography afforded Ph-TNI, NO_2Ph-TNI, and Ph_2NPh-TNI, respectively. Identity and purity of the synthesized compounds were confirmed with ^{1}H and ^{13}C NMR, APCI–HRMS, and GPC chromatograms; see Supporting Information for spectra and chromatograms.

Photophysical Properties. Experimental photophysical properties of the dyes are summarized in Table 1, while the spectra are shown in Figure S1. The solvent used were toluene, DMSO, and MeOH, as exemplars for nonpolar solvents, nonprotic polar solvents, and protic polar solvents, respectively. The parent NI exhibits an absorption band peaking at ~330 nm in toluene.[47] The introduction of the phenylthienyl group makes the absorption peak significantly red-shifted by ~65 nm to 398 nm (Ph-TNI). Further introduction of a nitro group has little influence on the peak position (392 nm for NO_2Ph-TNI). Introduction of a diphenylamino group, on the other hand, leads to a further red-shift by 42 nm, giving rise to the peak at 440 nm. The absorption maxima of these compounds are hardly affected by the solvent polarity on going from toluene to MeOH, as seen from the less than 8 nm changes.

Table 1. Photophysical Data for Ph-TNI, NO_2Ph-TNI, and Ph_2NPh-TNI

	Solvent	λ_{ab} /nm	$\varepsilon \times 10^{-4}$ /M^{-1} cm^{-1}	λ_{fl} /nm	$\Delta\nu$ /cm^{-1}	ϕ_f	τ_f /ns	k_r /ns^{-1}	k_{nr} /ns^{-1}
Ph-TNI	Toluene	398	1.53	493	5423	0.06 ± 0.02	0.21 ± 0.01	0.29 ± 0.10	4.28 ± 0.23
	DMSO	405	1.68	557	6738	0.43 ± 0.02	2.62 ± 0.05	0.16 ± 0.01	0.22 ± 0.01
	MeOH	403	1.78	572	7331	0.34 ± 0.02	2.53 ± 0.01	0.13 ± 0.01	0.26 ± 0.01
NO_2Ph-TNI	Toluene	392	2.95	479	4633	0.07 ± 0.02	0.22 ± 0.01	0.32 ± 0.09	4.23 ± 0.21
	DMSO	400	2.73	538	6413	0.17 ± 0.03	0.55 ± 0.00	0.31 ± 0.05	1.51 ± 0.05
	MeOH	393	2.11	531	6613	0.03 ± 0.00	0.20 ± 0.01	0.15 ± 0.01	4.85 ± 0.24
Ph_2NPh-TNI	Toluene	440	1.83	575	5336	0.56 ± 0.04	2.60 ± 0.05	0.22 ± 0.02	0.17 ± 0.02
	DMSO	445	1.52	–	–	<0.01	–	–	–

MeOH	447	1.35	–	–	<0.01	–	–	–

The parent NI emits fluorescence peaking at ~380 nm in toluene.[47] Compared to this, extension of the conjugate system as in Ph-TNI results in a large red shift in the fluorescence, which has a peak at 493 nm. Further introduction of a nitro group (NO_2Ph-TNI) slightly reduces this effect, resulting in the fluorescence peaking at 479 nm. Introduction of a diphenylamino group, on the other hand, results in a very large red shift, resulting in the fluorescence peaking at 575 nm.

In contrast to the absorption, the fluorescence from these compounds are very sensitive to the solvent polarity both in terms of the transition energy and the quantum yield. For Ph-TNI, the fluorescence red shifts on going from toluene (493 nm) to DMSO (557 nm), and further to MeOH (572 nm). For NO_2Ph-TNI, the fluorescence red shifts on going from toluene (479 nm) to DMSO (538 nm), but a slight blue shift is observed on going from DMSO to MeOH (531 nm). For Ph_2NPh-TNI, the solvent dependent shift was not clearly observed because this compound shows little fluorescence in DMSO and in MeOH. This point, therefore, was investigated in a different solvent system as discussed later. It is noted that each of these compounds exhibits a broad, structureless fluorescence band and none of them showed a dual fluorescence.[48-49] The absence of dual fluorescence is consistent with the single component exponential decays for these compounds in time-resolved fluorescence measurements as described later.

General solvent effects may be approximated by Onsager's reaction field model, in which a dipole is placed at the center of a vacuum cavity in a homogeneous dielectric medium.[50-51] The absorption (ν_{ab}) and fluorescence (ν_{fl}) frequencies in this treatment are expressed by eqs 2 and 3,

$$h\nu_{ab} = h\nu_{ab}^{0} - \Delta f \frac{2\mu_G(\mu_E - \mu_G)}{a^3} \quad (2)$$

$$h\nu_{\mathrm{fl}} = h\nu_{\mathrm{fl}}^{0} - \Delta f \frac{2\mu_{\mathrm{E}}(\mu_{\mathrm{E}} - \mu_{\mathrm{G}})}{a^{3}} \tag{3}$$

where Δf is the orientation polarizability, which is defined in eq 4.

$$\Delta f = \frac{\varepsilon - 1}{2\varepsilon + 1} - \frac{n^{2} - 1}{2n^{2} + 1} \tag{4}$$

Here, h is the Planck constant, ν_{ab}^{0} and ν_{fl}^{0} are the absorption and fluorescence frequency in the vacuum, respectively, ε is the dielectric constant of the solvent, n is the refractive index of the solvent, μ_{G} and μ_{E} are the dipole moments of the molecule in the ground and in the excited states, respectively, and a is the radius of the cavity.[52] The values of Δf of solvents used in this study are 0.013, 0.263, and 0.308 for toluene, DMSO, and MeOH, respectively. It should be noted that these equations hold for molecules whose dipole moment in the ground state and that in the excited state are oriented in the same direction. The assumption is likely to be valid for Ph-TNI and Ph_2NPh-TNI because the molecular structures, i.e., π-acceptor and donor-π-acceptor motifs, respectively, are fairly straightforwardly related to polarization. However, the polarization direction, in the ground state as well as in the excited state, is not obvious for NO_2Ph-TNI because of the acceptor–π-acceptor motif. The sensitivity of ν_{ab} and ν_{fl} on Δf is represented by the coefficients of Δf in eqs 2 and 3, respectively. Therefore, the observation that ν_{ab} is almost insensitive to the difference in Δf but that ν_{fl} becomes smaller with increasing Δf implies qualitatively that the coefficient of Δf in eq 2 is small whereas that in eq 3 is large. This means that the ratio $\mu_{\mathrm{E}}/\mu_{\mathrm{G}}$ is significantly larger than one; the excited-state dipole moments are significantly larger than the ground-state dipole moment for Ph-TNI and Ph_2NPh-TNI.

The dependence of the fluorescence quantum yield ϕ_f on the solvent is very characteristic to the respective compound under study. Ph-TNI is weakly fluorescent in the nonpolar solvent (0.07±0.02 in toluene) but strongly fluorescent in polar solvents (0.43±0.02 in DMSO; 0.34±0.02 in MeOH) whether the solvent is protic or nonprotic. NO_2Ph-TNI is weakly fluorescent irrespective of the solvent. Ph_2NPh-TNI is highly fluorescent in the nonpolar solvent (0.56±0.04 in toluene) but nearly nonfluorescent in polar solvents (<0.01 in DMSO, MeOH) whether the solvent is protic or nonprotic. The ϕ_f is expressed in eq. 5,

$$\phi_f = \frac{k_r}{k_r + k_{nr}} \tag{5}$$

where k_r and k_{nr} are the radiative and nonradiative decay rate constants from the singlet excited state, respectively. Thus a change in quantum yield can be ascribed to a change either in k_r or k_{nr}. These rate constants can be evaluated by measuring the excited-state (fluorescence) lifetime τ_f in addition to the quantum yield as indicated by eqs 6 and 7.

$$k_r = \frac{\phi_f}{\tau_f} \tag{6}$$

$$k_{nr} = \frac{1 - \phi_f}{\tau_f} \tag{7}$$

We performed the time-resolved fluorescence measurements to obtain the lifetimes. Every trace could be fitted by a single exponential decay with χ^2 values in a range of 1.05–1.56. The data thus obtained are shown in Figure S2 and the results are summarized in Table 1.

For Ph-TNI, it is now clear that the major reason for the increase of ϕ_f on going from nonpolar to polar solvent is mainly due to a decrease in k_{nr}. The k_{nr} for Ph-TNI decreases nearly 20-fold from 4.28±0.23 in toluene to 0.22±0.01 in DMSO and 0.26±0.01 in MeOH. For NO_2Ph-TNI,

changes in k_r and k_{nr} are both modest. For Ph_2NPh-TNI, the fluorescence in DMSO and in MeOH were so weak that the determination of k_r and k_{nr} was impossible in these solvents. Hence, the polarity dependence of k_r and k_{nr} for Ph_2NPh-TNI was examined separately as described later.

Similar decrease in k_{nr} on going from nonpolar to polar environment has been observed for the parent NI without an extended π system as well.[35,36] The energies of the lowest $^1\pi,\pi^*$ state and the lowest $^1n,\pi^*$ state are quite close for the parent NI.[39] On going from nonpolar to polar medium, the energy of the $^1\pi,\pi^*$ is lowered, while the energy of the $^1n,\pi^*$ state is raised, because the $^1\pi,\pi^*$ state is more stabilized than the ground state by polar solvents and the opposite is the case for the $^1n,\pi^*$ state. As a result, as the solvent polarity increases, the gap between the $^1n,\pi^*$ state and the $^1\pi,\pi^*$ state widens. The literature agrees up to this point. As a consequence of the widened gap, some authors, as the reason for the increase of ϕ_f in more polar solvents, invoked less facile intersystem crossing due to the less contribution of the $^1n,\pi^*$ state to the first singlet excited state (S_1),[36] while others invoked a smaller proximity effect.[40] The proximity effect is a nuclear motion-mediated coupling of the upper and lower electronic states, the $^1n,\pi^*$ and $^1\pi,\pi^*$ states in this particular case.[38] When the energies between the two electronic states are closer, the lower state potential curve becomes wider due to the vibronic interaction. Consequently, the Franck-Condon factor with the ground state becomes larger and hence k_{nr} also becomes larger. These considerations may also be applied for Ph-TNI, because the S_1 is a $^1\pi,\pi^*$ state with some charge transfer character, which is more stabilized in more polar solvents, resulting in a widened gap between this $^1\pi,\pi^*$ state and an upper lying $^1n,\pi^*$ state. It should be noted, however, that the gap between the $^1n,\pi^*$ state and the $^1\pi,\pi^*$ state is much wider already in the vacuum or in nonpolar solvents in the case of Ph-TNI than in the parent NI; see below in the section of DFT

calculations. Apart from the solvent polarity-dependent widening of the gap between the ^{1}n,π* and ^{1}π,π* states, an additional possibility of the solvent dependent change in k_{nr} is that the height of the energy barrier on excited state potential energy surfaces is solvent dependent.[53] This barrier separates strongly emitting planar geometry and a low emitting, twisted geometry. For Ph-TNI, the potentially rotatable bonds are the phenyl–thienylene bond and the thienylene–naphthalimide bonds.

To probe more accurately the effects of the solvent polarity on the photophysical behaviors of these compounds, the solvent polarity was incrementally changed by using a mixed solvent system consisting of 1,4-dioxane (ε = 2.25; n = 1.42) and MeCN (ε = 37.5; n = 1.34) and wavenumbers, $\bar{\nu}_{ab}$ and $\bar{\nu}_{fl}$, were recorded. The dielectric constants and the refractive indices of a binary mixture, which are needed for obtaining Δf values, are approximated by eqs 8 and 9, respectively,[54]

$$\varepsilon_{binary} = x_1\varepsilon_1 + x_2\varepsilon_2 \quad (8)$$

$$n_{binary} = \sqrt{x_1 n_1^2 + x_2 n_2^2} \quad (9)$$

where x_1 and x_2 are the mole fractions of solvent 1 and solvent 2, respectively.

The results are summarized as the Lippert-type plot in Figure 2a, in which wavenumbers are plotted in place of frequencies in eqs 2 and 3. All data are fitted on straight lines quite well, demonstrating that the simple Onsager model is good enough to explain the polarization dependent absorption and fluorescence changes. The absorption wavenumbers for all the compounds show slightly negative slopes, while the fluorescence wavenumbers for all the compounds show more pronounced negative slopes. A particularly large negative slope is observed for Ph_2NPh-TNI. These observations indicate that the fluorescence is due to ^{1}π,π*

transition with charge transfer character, whose contribution is particularly large for Ph_2NPh-TNI. These results are consistent with the solvent-dependent behaviors in toluene, DMSO, and MeOH described above.

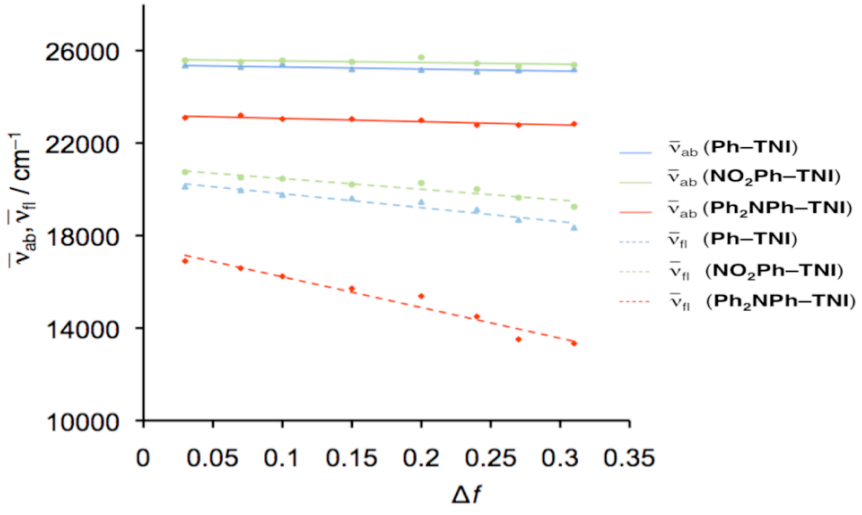
26000
22000
18000
14000
10000
$\bar{\nu}_{ab}, \bar{\nu}_{fl}$ / cm^{-1}
0
0.05
0.1
0.15
0.2
0.25
0.3
0.35
Δf
$\bar{\nu}_{ab}$ (Ph–TNI)
$\bar{\nu}_{ab}$ (NO$_2$Ph–TNI)
$\bar{\nu}_{ab}$ (Ph$_2$NPh–TNI)
$\bar{\nu}_{fl}$ (Ph–TNI)
$\bar{\nu}_{fl}$ (NO$_2$Ph–TNI)
$\bar{\nu}_{fl}$ (Ph$_2$NPh–TNI)

(a)

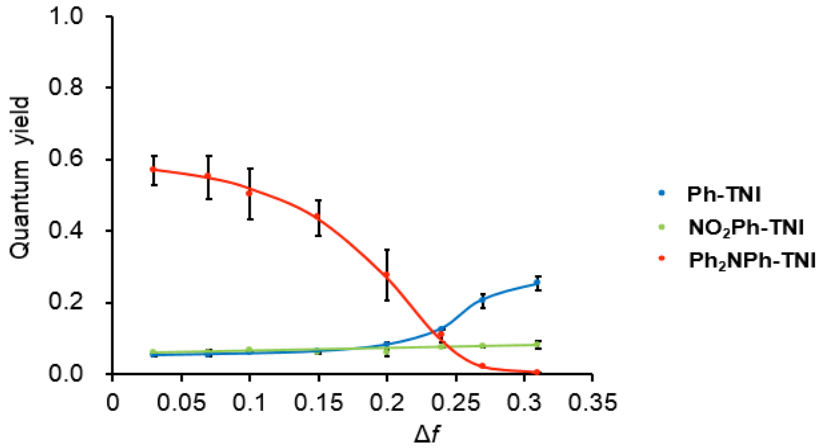
1.0
0.8
0.6
0.4
0.2
0.0
Quantum yield
0
0.05
0.1
0.15
0.2
0.25
0.3
0.35
Δf
Ph-TNI
NO$_2$Ph-TNI
Ph$_2$NPh-TNI

(b)

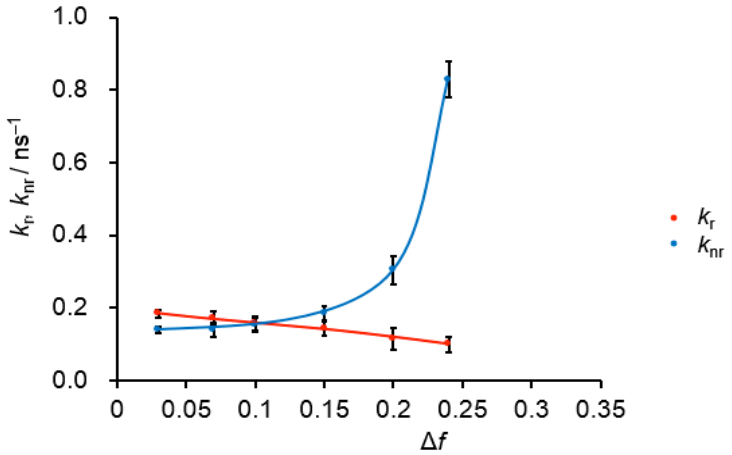
1.0
0.8
0.6
0.4
0.2
0.0
k_r, k_{nr} / ns^{-1}
0
0.05
0.1
0.15
0.2
0.25
0.3
0.35
Δf
k_r
k_{nr}

(c)

Figure 2. Dependence of photophysical properties on the orientation polarization Δf in a binary solvent system consisting of 1,4-dioxane and MeCN. (a) Absorption and fluorescence maxima. (b) Quantum yields. (c) Radiative and nonradiative rate constants for Ph_2NPh-TNI.

The dependence of the fluorescence quantum yield on Δf is shown in Figure 2b. The quantum yield increases as the Δf increases for Ph-TNI, while the quantum yield is consistently low over the range of Δf investigated for NO_2Ph-TNI. The dependence of fluorescence quantum yield on solvent polarity becomes now clear for Ph_2NPh-TNI whose fluorescence is extremely weak in DMSO and MeOH as described earlier. The quantum yield, starting from a high value of ca. 0.6 in 1,4-dioxane, gradually decreases as Δf increases, down to near zero values at $\Delta f > 0.25$. To see whether this decrease is due to changes in the rate of radiative process or the nonradiative process, k_r and k_{nr} are plotted in Figure 2c. While k_r decreases as Δf increases, a more prominent increase in k_{nr} is apparent particularly at a large Δf region as the major reason for the decrease of fluorescence quantum efficiency. Similar behaviors were also observed for *N*,*N*-dialkyl-4-amino-1,8-naphthalimides, in which a dialkylamino group is directly introduced onto the 1,8-naphthalimide core.[41] The fluorescence from these parent compounds decreases on going from nonpolar to polar solvent. The mechanism behind this behavior is not clear even for the parent *N*,*N*-dialkyl-4-amino-1,8-naphthalimides. It is certain that the excited state is the strongly charge-transferred state and hence is more stabilized in more polar solvents, as manifested in the negative slope in the Lippert-type plot for $\bar{\nu}_F$ of Ph_2NPh-TNI. We just make a general remark that the lower the energy of an excited state, k_{nr} becomes larger, which is in accord with the energy-gap law.[55]

Redox Properties. In addition to photophysical properties, redox properties of fluorophores are important particularly for this class of compounds, because they could be used for photoinduced electron-transfer sensors[13-14] and DNA oxidation.[11-12] The cyclic voltammograms are presented in Figure 3. For Ph-TNI, two reduction waves appear at –1.59 V (vs ferrocene/ferricenium) and –2.01 V, while an oxidation wave appears peaking at +1.17 V. The reductions are reversible but the oxidation is irreversible. Each redox wave for NO_2Ph-TNI (–1.46 V and +1.63 V) is observed at more positive potentials than the corresponding wave for Ph-TNI reflecting the electron withdrawing nature of the nitrophenyl substituent, except for the second reduction wave, which was not observed under our conditions. The oxidation waves for Ph_2NPh-TNI (+0.50 V and +1.00 V) appear at less positive potentials than that for Ph-TNI, reflecting the electron-donating nature of the triphenylamine unit. Both of these waves are now (quasi)reversible. The reduction waves for Ph_2NPh-TNI (–1.58 V and –2.17 V), however, appear at potentials almost the same as those for Ph-TNI. In general, it is noticed from the voltammograms that the differences for the reduction potentials among these compounds are quite small and the effect of substituents are more manifested in the oxidation potentials.

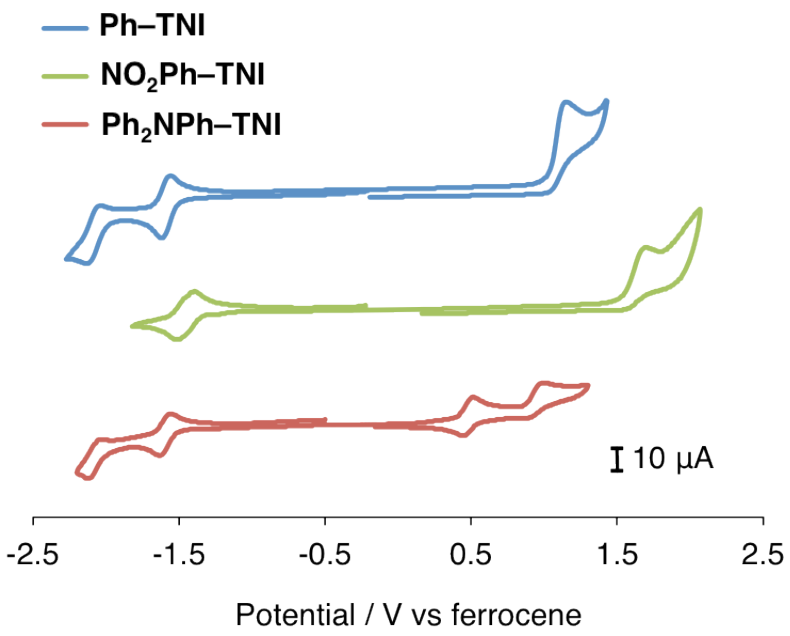

Figure 3. Cyclic voltammograms. Measurement conditions are as follows. Sample concentration: 1 mM; electrolyte: 0.1 M $N(Bu)_4PF_6$ solution in MeCN; working electrode: Pt; counter electrode: Pt; quasi-reference electrode: Ag; scan rate: 100 mV s^{-1}. The potentials are given versus the internal ferrocene/ferricenium couple.

DFT Calculations. DFT calculations were performed to probe the electronic structures of these molecules both in the ground state and in the excited state. For the calculations, the substituent on the imide nitrogen (the 2,5-*t*-butylphenyl group) was replaced by a hydrogen atom to reduce the computation time. The ground state geometries were optimized using the B3LYP hybrid functional[56] combined with the 6-31+G* basis set, which contains the diffuse functions and the polarization functions for atoms other than hydrogen. We then computed the transition energies to the singlet excited electronic states on these ground-state geometries with TDDFT. We compared the results of calculations obtained by using some different functionals, i.e., B3LYP,[56] CAM-B3LYP,[57] and BMK[58] with the experimental data. The experimental absorption

maxima for Ph-TNI, NO_2Ph-TNI, and Ph_2NPh-TNI are 398, 392, and 440 nm in toluene, respectively (Table 1). The B3LYP/6-31+G* gave the values of 437, 425, and 555 nm, respectively, significantly underestimating the transition energies (2000–4700 cm^{-1}), particularly for Ph_2NPh-TNI, which is expected to have a large charge transfer character. The poor performance of B3LYP, with its low fraction (20%) of the Hartree–Fock exchange, for charge transfer excitations is well known.[59-60] Increasing the fraction of the Hartree-Fock exchange in a range-separated manner where the fraction of Hartree-Fock exchange depends on the electron–electron distance (e.g., CAM-B3LYP) or in a manner through the kinetic energy density (e.g., BMK) alleviates the problem. For the present molecules, the CAM-B3LYP/6-31+G* gave the values of 361, 359, and 390 nm as the transition wavelengths, respectively, significantly overestimating the energies (2300–2900 cm^{-1}). The BMK/6-31+G*, on the other hand, gave reasonable values of 377, 371, and 429 nm, respectively, with deviations from experiments being in a range of 500–1400 cm^{-1}. Accordingly, we decided to use the BMK functional in the following excited state calculations. The HOMOs and LUMOs obtained by BMK/6-31+G* are displayed in Table 2 and the transition energies and the oscillator strengths are superimposed on the experimental spectra in toluene in Figure 4.

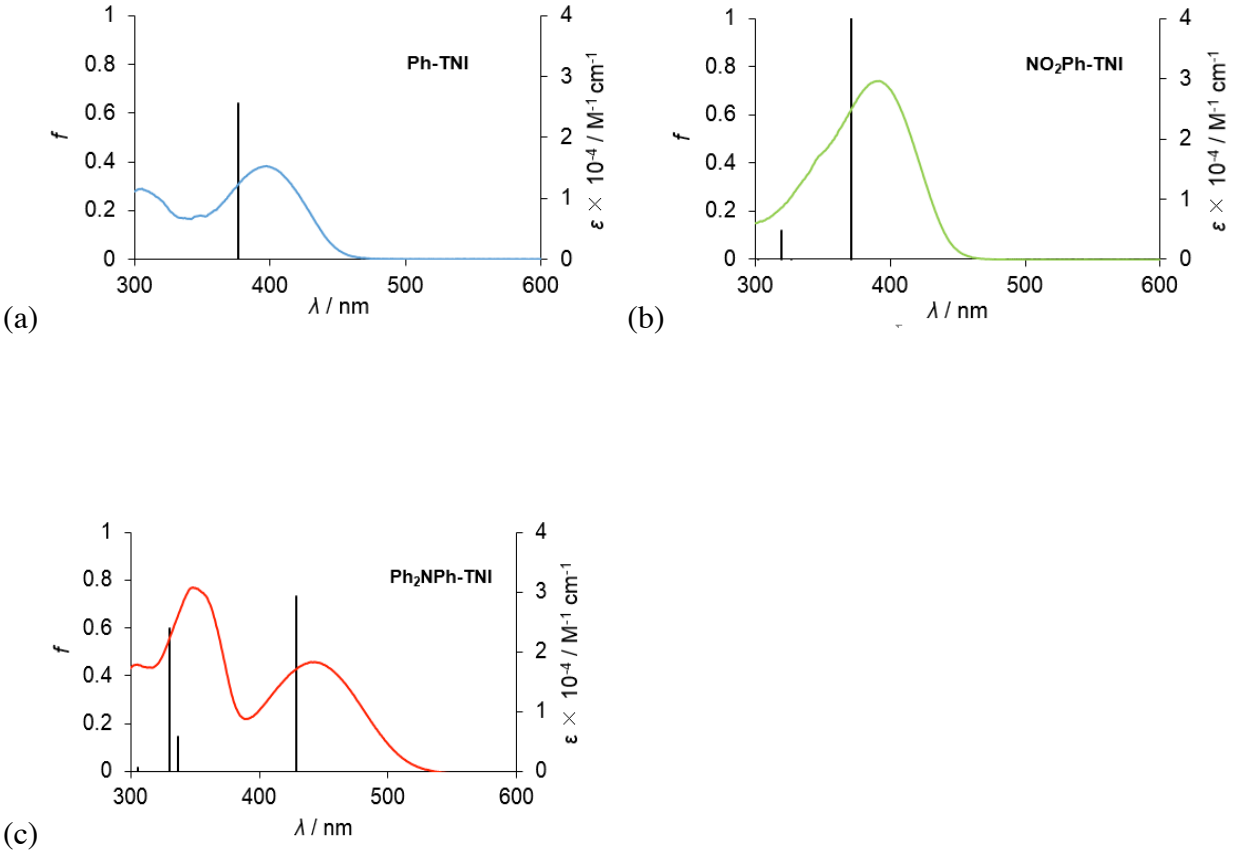

Figure 4. Oscillator strengths and absorption spectra. The oscillator strengths were obtained by TDDFT calculations (BMK/6-31+G*) and the spectra are those in toluene. (a) Ph-TNI. (b) NO_2Ph-TNI. (c) Ph_2NPh-TNI.

According to the TDDFT calculations, the lowest singlet excited states for all these compounds have predominantly the HOMO→LUMO configuration. Thus, the S_1 on the vertical excitation are $^1\pi,\pi^*$ states. For Ph-TNI, the HOMO is largely delocalized over the entire π system, while the LUMO is mainly localized on the naphthalimide unit. Therefore, the lowest singlet excited state, which appears at 377 nm according to the TDDFT calculations and at 398 nm in the experiment in toluene, is a $^1\pi,\pi^*$ state with an appreciable charge transfer nature. The

charge transfer nature is visualized by the difference map which is also displayed in Table 2. The map was made by plotting the difference between the squares of the coefficients of the LUMO and those of the HOMO. It is clearly seen from the difference map that the charge moves from the phenylthienyl unit to the naphthalimide unit on going from the ground state to the S_1.

Table 2. LUMO, HOMO, and Difference Maps According to DFT (BMK/6-31+G*)

	Ph–TNI	NO_2Ph–TNI	Ph_2NPh–TNI
LUMO	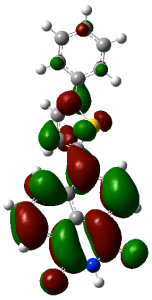	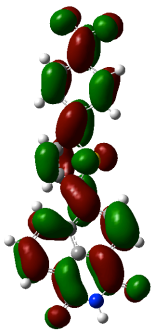	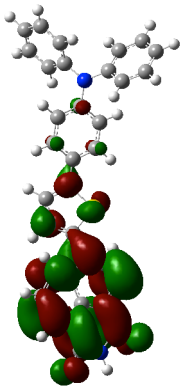
HOMO	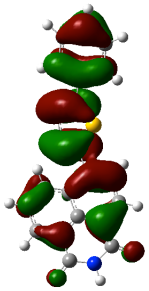	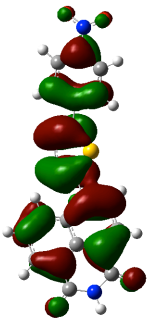	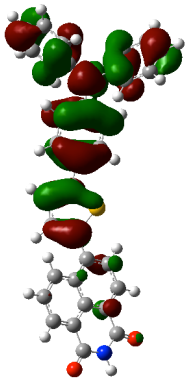
$S_0 \rightarrow S_1$ [a]	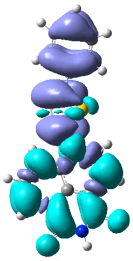	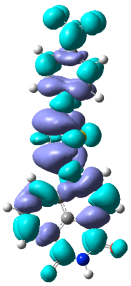	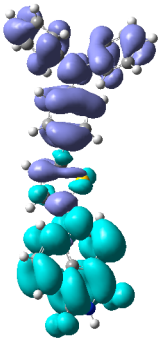

[a] On going from the S_0 state to the S_1 state, charge moves from the purple to the sky blue regions.

For NO_2Ph-TNI, both the HOMO and LUMO are delocalized over the entire π system. It is an interesting question which group withdraws electrons more strongly in this molecule, the nitro group or the dicarboximide group. The calculated dipole moment of the ground state is oriented

nearly perpendicularly with respect to the molecule's long axis, which indicates that the groups at both ends of the molecule withdraw electrons nearly equally. This is also the case for the S_1. Both of the nitro group and the imide moiety at both ends of the molecule pull the electrons nearly equally, as seen from the difference map. According to the TDDFT calculations, the lowest singlet excited $^1\pi,\pi^*$ state is located at 371 nm.

For Ph_2NPh-TNI, a significant charge-transfer nature in the HOMO→LUMO transition is apparent. The HOMO is localized on the diphenylaminophenylthienyl unit, while the LUMO is mostly localized on the naphthalimide moiety. Therefore, the HOMO→LUMO transition is a $^1\pi,\pi^*$ transition with a large contribution of charge transfer. The charge transfer character is clearly seen from the difference map, in which electrons move from the triphenylamine unit to the naphthalimide unit. According to the TDDFT calculations, this transition to the S_1 is located at 429 nm.

The same set of calculations were performed on the parent NI as a reference to highlight the effects of the extended π system of the present three dyes. The HOMO and LUMO of NI are π and π* orbitals according to BMK/6-31+G*//B3LYP/6-31+G*. The n-orbital mainly localized on the carbonyl oxygens is the HOMO–2 orbital lying below the HOMO by 1.17 eV. According to the TDDFT BMK/6-31+G* calculations, the S_1 is a $^1\pi,\pi^*$ state, in which an electron in the HOMO is excited to the LUMO, with the transition at 308 nm. The second singlet excited state, which is a $^1n,\pi^*$ state with a major configuration of HOMO–2 → LUMO, lies very close in energy (298 nm) to the S_1. This result indicating the closely separated $^1\pi,\pi^*$ and $^1n,\pi^*$state agrees with calculations in the literature.[39]

To gain more insight into the excited states, we carried out TDDFT calculations focusing on the excited states in different solvents. First, we optimized the excited state structures in toluene, DMSO, and MeOH starting with the geometries optimized in vacuum as the initial input structures. This was done by employing the polarizable continuum model and the self-consistent reaction field options, which are implemented in the Gaussian 09 package with TDDFT (BMK/6-31G). In short, the excited state in solution was found to be more planar than the ground state in vacuum (B3LYP/6-31+G*). More specifically, the dihedral angle between the thienylene ring and the naphthalimide plane is 47–50° for each of the three thienylnapththalimide compounds in the ground state in vacuum, while this angle is reduced to 21–28° in the excited state for every compound in every solvent. The dihedral angles between the thienylene ring and the phenylene ring are 23–29° in the ground states in vacuum, while these angles are 3–5° in the excited states in solution. Next, single point calculations were done on the optimized structure using the state specific model with the key word *ExternalIteration* in the Gaussian packege.[61-62] This model calculates the self-consistent reaction field with equilibrium solvation, in which both the fast and slow components of the solvent polarization, which correspond to the electronic and orientation polarization, respectively, are in equilibrium with the geometrical and electronic structures of the solute molecule in the excited state.

Excited-state energies thus obtained are displayed in Figure 5. For NI, the lowest singlet excited state is a $^1\pi,\pi^*$ state and the second lowest singlet excited state is a $^1n,\pi^*$ state. These two states are separated by 0.28 eV in toluene. Upon increasing the solvent polarity from toluene to DMSO or MeOH, the $^1\pi,\pi^*$ state is stabilized while the $^1n,\pi^*$ state is destabilized, resulting in the widened gap up to 0.42 eV. Although the energies in DMSO and in MeOH are quite close, we should note that specific interactions, particularly hydrogen bonding, are not taken into

account in the present model calculations. As discussed above, the larger separation in energy between the $^1\pi,\pi^*$ state and the $^1n,\pi^*$ states in a more polar environment will lead to a lower nonradiative decay rate whether it is due to a less facile intersystem crossing or due to a smaller proximity effect.

For the present three thienylnaphthalimide compounds, the general characteristics in the solvent dependency are similar to those for NI; (i) the lowest singlet excited state S_1 is a $^1\pi,\pi^*$ state, (ii) the S_1 gets lower in energy in more polar solvents, (iii) the $^1n,\pi^*$ state gets higher in energy in more polar solvent. However, the S_1 energies of the present three compounds are much lower in energy than that of NI, resulting in much wider gaps between the $^1n,\pi^*$ and $^1\pi,\pi^*$ states even in less polar toluene. Experimentally, the solvent dependence of fluorescence intensity is the same for NI[35-37, 40] and Ph-TNI; more intense fluorescence in more polar solvents. Thus, the argument applied to NI may also be applied to Ph-TNI, with a caveat that the gap between the $^1n,\pi^*$ and $^1\pi,\pi^*$ states is already wide in toluene: less involvement of $^1n,\pi^*$ states in more polar solvents leads to less nonradiative decay rates. For NO_2Ph-TNI, a $^1n,\pi^*$ state involving not the carbonyl moieties but the nitro group is found as the S_2 or S_3 states depending on the solvent. The presence of this low-lying $^1n,\pi^*$ state could prompt the nonradiative process, which may account for the relatively large nonradiative decay rates and low fluorescence yields for NO_2Ph-TNI. For Ph_2NPh-TNI, the S_1 state is even lower in energy than the other compounds. Just contrary to NI and Ph-TNI, the nonradiative decay rates for Ph_2NPh-TNI as well as for *N*,*N*-dialkyl-4-amino-1,8-naphthalimide[39-42] increase in more polar environments (Figure 2c). As described earlier, no definite mechanism for this behavior seems to have been presented even for the simpler *N*,*N*-dialkyl-4-amino-1,8-naphthalimide in the literature. Further complication arises in the case of

Ph_2NPh-TNI, because this molecule has five rotatable bonds. While the present optimization was done for the nearly planar conformation, the excited-state molecule may sweep over the potential energy surface and could find effective nonradiative paths to the ground state and the height of the relevant energy barrier may depend on the solvent.[63]

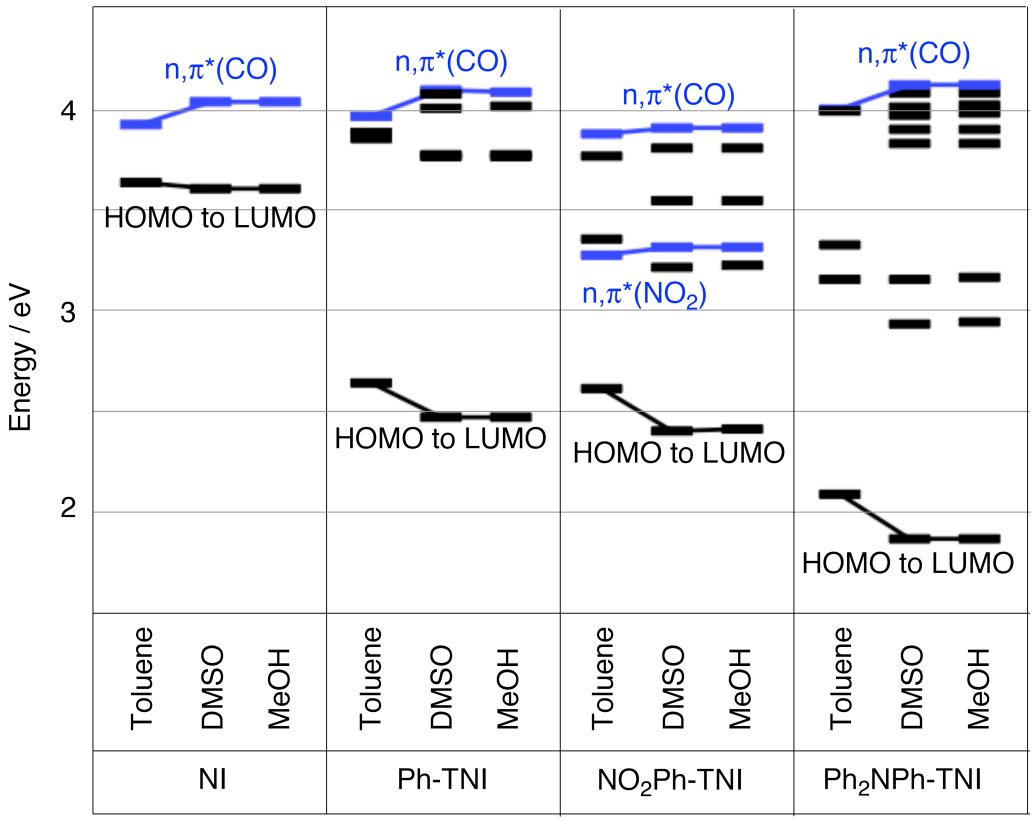

Figure 5. Excited state energies in solvents obtained from a state specific model in TDDFT (BMK/6-31G). Excited states from S_1 up to the ^{1}n,π* (CO) excited state are shown. Black bars indicate ^{1}π,π* states and blue bars indicate ^{1}n,π* states.

Photostability. Although it is often advertized that naphthalimide dyes are stable, concrete data for stability are rarely reported. Here we compare the photostability of our newly

synthesized dyes with those of known commercial dyes. A broad band of visible light in a range of 400–700 nm was continuously irradiated from a 100 W Xe-lamp to 1 μM solutions, during which time the absorption and fluorescence spectra were monitored. The irradiation was carried out in air. The results are presented in Figure 6. As a representative example for nonpolar solvents, toluene was chosen. Coumarin 343, which has an absorption band over 370–470 nm, was used as a reference for the experiments in toluene. One hour after under our irradiation conditions, when the absorbance as well as the fluorescence of the coumarin 343 dye diminished to about 20% of the original values, no sign of degradation was observed for the present three dyes (Figures 5a and 5b). As a representative example for polar solvents, MeCN was chosen and fluorescein isothiocyanate, which is one of the most commonly used fluorescent labels (λ_{max} ~500 nm), was used as a reference. One hour after under our irradiation conditions, when the absorbance as well as the fluorescence of fluorescein isothiocyanate diminished to ~15% of the original values, no sign of degradation was observed for Ph-TNI and Ph_2NPh-TNI. Note that only the absorption was monitored for Ph_2NPh-TNI, because this dye is almost nonfluorescent in MeCN as described earlier. On the other hand, NO_2Ph-TNI showed changes in absorption and fluorescence spectra during the first 20 minutes of irradiation. The absorption changes were accompanied by an isosbestic point. After 20-minute irradiation, both the new absorption and fluorescence spectra remained constant. Absorption maximum was slightly red-shifted by 3 nm from that of the original NO_2Ph-TNI, while the fluorescence maximum was red-shifted by 30 nm. Similar changes were also observed when a solution purged with Ar was irradiated. These observations suggest that NO_2Ph-TNI has changed into a new, stable fluorescent species upon irradiation, although we have not identified the product at this moment.

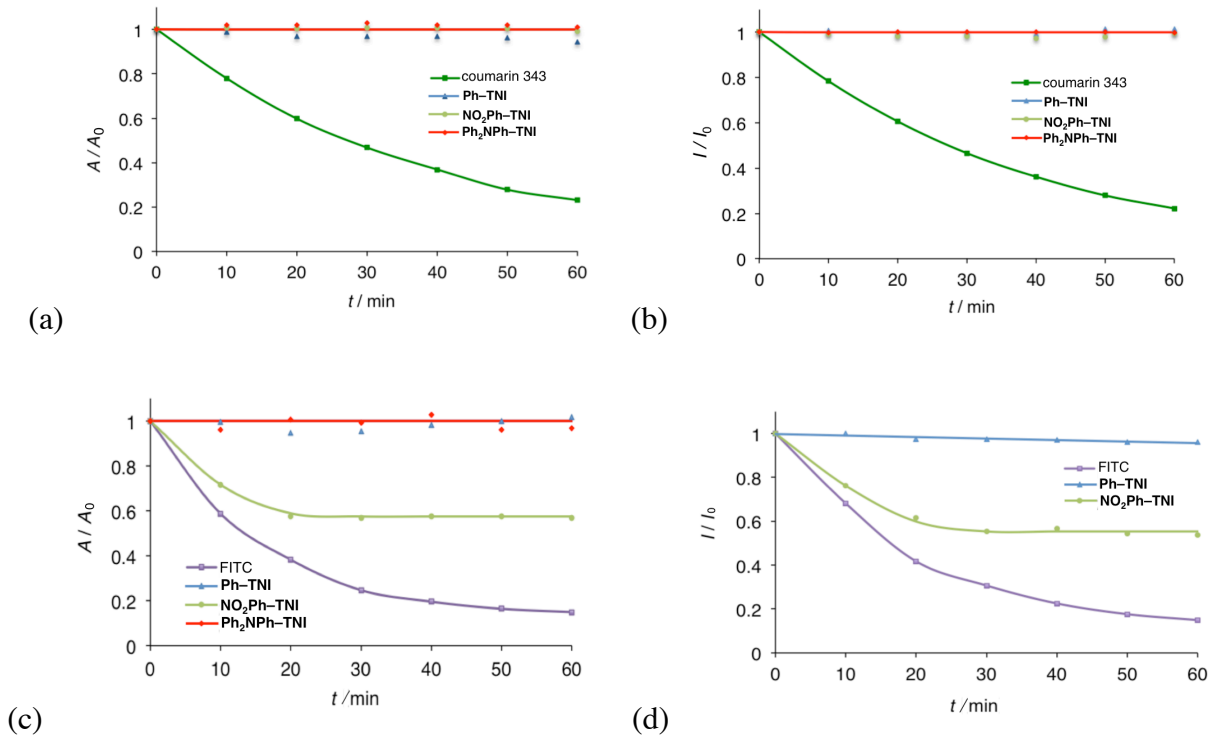

Figure 6. Stability of dyes under light irradiation (100 W Xe lamp, 400–700 nm). Light was irradiated to a solution of 1 μM dye in toluene (a and b) and in MeCN (c and d), during which time the relative absorbance at λ_{ab} (a and c) and the fluorescence intensity at λ_{fl} (b and d) were recorded.

CONCLUSIONS

We have prepared naphthalimide fluorescent dyes whose π system is extended via a thienylene spacer by additional aromatic unit with or without an electron-withdrawing or electron-donating substituent. By extending the π system, both absorption and fluorescence exhibit significant red-shifts. The lowest energy transitions are $^1\pi,\pi^*$ transitions with a significant charge transfer character, according to TDDFT calculations. The solvent dependent photophysics were

investigated. Briefly, the fluorescence quantum yield of Ph-TNI, which is terminated with a phenyl group without any electron-withdrawing or electron-donating group, is low in nonpolar media but quite high in polar media. In sharp contrast, the fluorescence quantum yield of Ph_2NPh-NTI, which is terminated by an electron donating group, is as high as $\phi \sim 0.6$ in nonpolar media but becomes extremely low in polar media. We found that these behaviors are mainly ascribed to the solvent-dependent changes in nonradiative decay rate rather than to those in the radiative rate. The photostability of these dyes, except for NO_2Ph-TNI, is much higher than archetypal dyes such as a coumarin dye and a fluorescein dye. The current active researches on the parent NI dyes for applications to DNA-oxidation,[11-12] sensing,[13-27] and organic light-emitting diodes[28] are manifestations of the bright prospect of this class of dyes. The significantly red-shifted absorption and fluorescence bands exhibited by the dyes presented here as compared with the parent dyes, which offers additional advantages when aiming at practical applications, combined with the excellent photostability, make these dyes very promising as a scaffold for further derivatization for various applications.

ASSOCIATED CONTENT

S Supporting Information

The complete author list for references, absorption and fluorescence spectra, time-resolved fluorescence traces, and characterization data for new compounds. This material is available free of charge via the Internet at http://pubs.acs.org.

AUTHOR INFORMATION

Corresponding Author

*E-mail: otsuki.joe@nihon-u.ac.jp.

Notes

The authors declare no competing financial interest.

ACKNOWLEDGEMENTS

We greatly acknowledge support for this work from the Nihon University "*N*." Research Project.

REFERENCES

(1) Pavlopoulos, T. G. Scaling of Dye Lasers with Improved Laser Dyes. *Prog. Quantum Electron.* **2002,** *26*, 193–224.

(2) Giepmans, B. N. G.; Adams, S. R.; Ellisman, M. H.; Tsien, R. Y. The Fluorescent Toolbox for Assessing Protein Location and Function. *Science* **2006,** *312*, 217–224.

(3) Finney, N. S. Combinatorial Discovery of Fluorophores and Fluorescent Probes. *Curr. Opin. Chem. Biol.* **2006,** *10*, 238–245.

(4) Ulrich, G.; Ziessel, R.; Harriman, A. The Chemistry of Fluorescent Bodipy Dyes: Versatility Unsurpassed. *Angew. Chem. Int. Ed.* **2008,** *47*, 1184–1201.

(5) Kim, B.-G.; Chung, K.; Kim, J. Molecular Design Principle of All-Organic Dyes for Dye-Sensitized Solar Cells. *Chem. Eur. J.* **2013,** *19*, 5220–5230.

(6) Banerjee, S.; Veale, E. B.; Phelan, C. M.; Murphy, S. A.; Tocci, G. M.; Gillespie, L. J.; Frimannsson, D. O.; Kelly, J. M.; Gunnlaugsson, T. Recent Advances in the Development of

1,8-Naphthalimide Based DNA Targeting Binders, Anticancer and Fluorescent Cellular Imaging Agents. *Chem. Soc. Rev.* **2013,** *42*, 1601–1618.

(7) Weil, T.; Vosch, T.; Hofkens, J.; Peneva, K.; Müllen, K. The Rylene Colorant Family—Tailored Nanoemitters for Photonics Research and Applications. *Angew. Chem. Int. Ed.* **2010,** *49*, 9068–9093.

(8) Otsuki, J.; Takaguchi, Y.; Takahashi, D.; Sugawa, K.; Kalimuthu, P.; Islam, A.; Han, L. Substituent Effects for Perylenedicarboxylic Anhydrides on the Performance of Dye-Sensitized Solar Cells: The Simpler, the Better. *Chem. Lett.* **2013,** *42*, 450–452.

(9) Otsuki, J.; Takaguchi, Y.; Takahashi, D.; Kalimuthu, P.; Singh, S. P.; Islam, A.; Han, L. Piperidine-Substituted Perylene Sensitizer for Dye-Sensitized Solar Cells. *Adv. OptoElectron.* **2011,** *2011*, 860486.

(10) Segura, J. L.; Herrera, H.; Bäuerle, P. Oligothiophene-Functionalized Naphthalimides and Perylene Imides: Design, Synthesis and Applications. *J. Mater. Chem.* **2012,** *22*, 8717–8733.

(11) Zhang, X.; Zhao, Z.; Mei, H.; Qiao, Y.; Liu, Q.; Luo, W.; Xia, T.; Fang, X. A Fluorescence Aptasensor Based on DNA Charge Transport for Sensitive Protein Detection in Serum. *Analyst* **2011,** *136*, 4764–4769.

(12) Li, Q.; Browne, W. R.; Roelfes, G. DNA Cleavage Activity of Fe(II)N4py under Photo Irradiation in the Presence of 1,8-Naphthalimide and 9-Aminoacridine: Unexpected Effects of Reactive Oxygen Species Scavengers. *Inorg. Chem.* **2012,** *50*, 8318–8325.

(13) Tian, H.; Gan, J.; Chen, K.; He, J.; Song, Q. L.; Hou, X. Y. Positive and Negative Fluorescent Imaging Induced by Naphthalimide Polymers. *J. Mater. Chem.* **2002,** *12*, 1262–1267.

(14) Li, Z.-Z.; Niu, C.-G.; Zeng, G.-M.; Liu, Y.-G.; Gao, P.-F.; Huang, G.-H.; Mao, Y.-A. A Novel Fluorescence Ratiometric pH Sensor Based on Covalently Immobilized Piperazinyl-1,8-Napthalimide and Benzothioxanthene. *Sens. Actuators B* **2006,** *114*, 308–315.

(15) Xu, Z.; Xiao, Y.; Qian, X.; Cui, J.; Cui, D. Ratiometric and Selective Fluorescent Sensor for Cu^{II} Based on Internal Charge Transfer (ICT). *Org. Lett.* **2005,** *7*, 889–892.

(16) Huang, J.; Xu, Y.; Qian, X. A Red-Shift Colorimetric and Fluorescent Sensor for Cu^{2+} in Aqueous Solution: Unsymmetrical 4,5-Diaminonaphthalimide with N-H Deprotonation Induced by Metal Ions. *Org. Biomol. Chem.* **2009,** *7*, 1299–1303.

(17) Singh, N.; Kaur, N.; McCaughan, B.; Callan, J. F. Ratiometric Fluorescent Detection of Cu(II) in Semi-Aqueous Solution Using a Two-Fluorophore Approach. *Tetrahedron Lett.* **2010,** *51*, 3385–3387.

(18) Satriano, C.; Sfrazzetto, G. T.; Amato, M. E.; Ballistreri, F. P.; Copani, A.; Giuffrida, M. L.; Grasso, G.; Pappalardo, A.; Rizzarelli, E.; Tomaselli, G. A. et al. A Ratiometric Naphthalimide Sensor for Live Cell Imaging of Copper(I). *Chem. Commun.* **2013,** *49*, 5565–5567.

(19) Dai, H.; Xu, H. A Water-Soluble 1,8-Naphthalimide-Based 'Turn on' Fluorescent Chemosensor for Selective and Sensitive Recognition of Mercury Ion in Water. *Bioorg. Med. Chem.* **2011,** *21*, 5141–5144.

(20) Kumaresan, D.; Thummel, R. P.; Bura, T.; Ulrich, G.; Ziessel, R. Color Tuning in New Metal-Free Organic Sensitizers (Bodipys) for Dye-Sensitized Solar Cells. *Chem. Eur. J.* **2009,** *15*, 6335–6339.

(21) Jiang, J.; Jiang, H.; Liu, W.; Tang, X.; Zhou, X.; Liu, W.; Liu, R. A Colorimetric and Ratiometric Fluorescent Probe for Palladium. *Org. Lett.* **2011,** *13*, 4922–4925.

(22) Lu, C.; Xu, Z.; Cui, J.; Zhang, R.; Qian, X. Ratiometric and Highly Selective Fluorescent Sensor for Cadmium under Physiological pH Range: A New Strategy to Discriminate Cadmium from Zinc. *J. Org. Chem.* **2007,** *72*, 3554–3557.

(23) Zhang, J. F.; Lim, C. S.; Bhuniya, S.; Cho, B. R.; Kim, J. S. A Highly Selective Colorimetric and Ratiometric Two-Photon Fluorescent Probe for Fluoride Ion Detection. *Org. Lett.* **2011,** *13*, 1190–1193.

(24) Ren, J.; Wu, Z.; Zhou, Y.; Li, Y.; Xu, Z. Colorimetric Fluoride Sensor Based on 1,8-Naphthalimide Derivatives. *Dyes Pigm.* **2011,** *91*, 442–445.

(25) Zhang, J. F.; Park, M.; Ren, W. X.; Kim, Y.; Kim, S. J.; Jung, J. H.; Kim, J. S. A Pellet-Type Optical Nanomaterial of Silica-Based Naphthalimide-DPA-Cu(II) Complexes: Recyclable Fluorescence Detection of Pyrophosphate. *Chem. Commun.* **2011,** *47*, 3568–3570.

(26) Zhang, J. F.; Kim, S.; Han, J. H.; Lee, S.-J.; Pradhan, T.; Cao, Q. Y.; Lee, S. J.; Kang, C.; Kim, J. S. Pyrophosphate-Selective Fluorescent Chemosensor Based on 1,8-Naphthalimide–DPA–Zn(II) Complex and Its Application for Cell Imaging. *Org. Lett.* **2011,** *13*, 5294–5297.

(27) Moro, A. J.; Cywinski, P. J.; Korsten, S.; Mohr, G. J. An ATP Fluorescent Chemosensor Based on a Zn(II)-Complexed Dipicolylamine Receptor Coupled with a Naphthalimide Chromophore. *Chem. Commun.* **2010,** *46*, 1085–1087.

(28) Gan, J.-A.; Song, Q. L.; Hou, X. Y.; Chen, K.; Tian, H. 1,8-Naphthalimides for Non-Doping OLEDs: The Tunable Emission Color from Blue, Green to Red. *J. Photochem. Photobiol. A* **2004,** *162*, 399–406.

(29) Jacquemin, D.; Perpète, E. A.; Scalmani, G.; Ciofini, I.; Peltier, C.; Adamo, C. Absorption and Emission Spectra of 1,8-Naphthalimide Fluorophores: A PCM-TD-DFT Investigation. *Chem. Phys.* **2010,** *372*, 61–66.

(30) Barbarella, G.; Melucci, M.; Sotgiu, G. The Versatile Thiophene: An Overview of Recent Research on Thiophene-Based Materials. *Adv. Mater.* **2005,** *17*, 1581–1593.

(31) Cao, Z.; Nandhikonda, P.; Penuela, A.; Nance, S.; Heagy, M. D. *N*-Aryl Arenedicarboximides as Tunable Panchromatic Dyes for Molecular Solar Cells. *Int. J. Photoenergy* **2010,** *2010*, 264643.

(32) Cao, J.-X.; Cheng, Y.-X.; Xie, Z.-Y.; Wang, L.-X.; Jing, X.-B.; Wang, F.-S. Synthesis and Characterization of Novel Blue Light-Emitting 1,8-Naphthalimide Derivatives. *Yingyong Huaxue* **2007,** *24*, 853–857.

(33) Wonneberger, H.; Pschirer, N.; Bruder, I.; Schöneboom, J.; Ma, C.-Q.; Erk, P.; Li, C.; Bäuerle, P.; Müllen, K. Double Donor-Thiophene Dendron-Perylene Monoimide: Efficient Light-Harvesting Metal-Free Chromophore for Solid-State Dye-Sensitized Solar Cells. *Chem. Asian J.* **2011,** *6*, 1744–1747.

(34) Zhengneng, J.; Najun, L.; Chuanfeng, W.; Huajiang, J.; Jianmei, L.; Qizhong, Z. Synthesis and Fluorescence Property of Some Novel 1,8-Naphthalimide Derivatives Containing a Thiophene Ring at the C-4 Position. *Dyes Pigm.* **2013,** *96*, 204–210.

(35) Barros, T. C.; Molinari, G. R.; Berci Filho, P.; Toscano, V. G.; Politi, M. J. Photophysical Properties of *N*-Alkylnaphthalimides and Analogs. *J. Photochem. Photobiol. A* **1993,** *76*, 55–60.

(36) Samanta, A.; Saroja, G. Steady State and Time-Resolved Studies on the Redox Behaviour of 1,8-Naphthalimide in the Excited State. *J. Photochem. Photobiol. A* **1994,** *84*, 19–26.

(37) Alexiou, M. S.; Tychopoulos, V.; Ghorbanian, S.; Tyman, J. H. P.; Brown, R. G.; Brittain, P. I. The UV-Visible Absorption and Fluorescence of Some Substituted 1,8-Naphthalimides and Naphthalic Anhydrides. *J. Chem. Soc. Perkin Trans. 2* **1990**, 837–842.

(38) Lim, E. C. Proximity Effect in Molecular Photophysics: Dynamical Consequences of Psudo-Jahn-Teller Interaction. *J. Phys. Chem. A* **1986,** *90*, 6770–6777.

(39) Kucheryavy, P.; Li, G.; Vyas, S.; Hadad, C.; Glusac, K. D. Electronic Properties of 4-Substituted Naphthalimides. *J. Phys. Chem. A* **2009,** *113*, 6453–6461.

(40) Dhar, S.; Roy, S. S.; Rana, D. K.; Bhattacharya, S.; Bhattacharya, S.; Bhattacharya, S. C. Tunable Solvatochromic Response of Newly Synthesized Antioxidative Naphthalimide Derivatives: Intramolecular Charge Transfer Associated with Hydrogen Bonding Effect. *J. Phys. Chem. A* **2011,** *115*, 2216–2224.

(41) Dmitruk, S. L.; Druzhinin, S. L.; Minakova, R. A.; Bedrik, A. I.; Uzhinov, B. M. Radiationless Deactivation of Excited Molecules of 4-Aminonaphthalimides. *Russ. Chem. Bull.* **1997,** *46*, 2027–2031.

(42) Yuan, D.; Brown, R. G. Enhanced Nonradiative Decay in Aqueous Solutions of Aminonaphthalimide Derivatives via Water-Cluster Formation. *J. Phys. Chem. A* **1997,** *101*, 3461–3466.

(43) Hamel, M.; Simic, V.; Normand, S. Fluorescent 1,8-Naphthalimides-Containing Polymers as Plastic Scintillators. An Attempt for Neutron–Gamma Discrimination. *React. Funct. Polym.* **2008,** *68*, 1671–1681.

(44) Fischer, M.; Georges, J. Fluorescence Quantum Yield of Rhodamine 6G in Ethanol as a Function of Concentration Using Thermal Lens Spectrometry. *Chem. Phys. Lett.* **1996,** *260*, 115–118.

(45) Rurack, K.; Spieles, M. Fluorescence Quantum Yields of a Series of Red and Near-Infrared Dyes Emitting at 600−1000 nm. *Anal. Chem.* **2011,** *83*, 1232-1242.

(46) Frisch, M. J.; Trucks, G. W.; Schlegel, H. B.; Scuseria, G. E.; Robb, M. A.; Cheeseman, J. R.; Scalmani, G.; Barone, V.; Mennucci, B.; Petersson, G. A. et al. *Gaussian 09*, Revision D.01, Gaussian, Inc.: Wallingford CT, 2013.

(47) Prezhdo, O. V.; Uspenskii, B. V.; Prezhdo, V. V.; Boszczyk, W.; Distanov, V. B. Synthesis and Spectral-Luminescent Characteristics of *N*-Substituted 1,8-Naphthalimides. *Dyes Pigm.* **2007,** *72*, 42–46.

(48) Nandhikonda, P.; Begaye, M. P.; Cao, Z.; Heagy, M. D. Discovery of Dual Fluorescent 1,8-Naphthalimide Dyes Based on Balanced Seesaw Photophysical Model. *Chem. Commun.* **2009**, 4941–4943.

(49) Ganin, E. V.; Masunov, A. E.; Siminel, A. V.; Fonari, M. S. Preparation, Characterization, and Electronic Structure of Asymmetric Isonaphthalimide: Mechanism of Dual Fluorescence in Solid State. *J. Phys. Chem. C* **2013,** *117*, 18154–18162.

(50) Lippert, V. E. Spektroskopische Bistimmung des Dipolmomentes aromatischer Verbindungen im ersten angeregten Singulettzustand. *Z. Electrochem.* **1957,** *61*, 962–975.

(51) Mataga, N.; Kaifu, Y.; Koizumi, M. Solvent Effects Upon Fluorescence Spectra and the Dipolemoments of Excited Molecules. *Bull. Chem. Soc. Jpn.* **1956,** *29*, 465–470.

(52) Lakowicz, J. R. *Principles of Fluorescence Spectroscopy*, 3rd ed.; Springer: New York, 2006.

(53) Moreshead, W. V.; Przhonska, O. V.; Bondar, M. V.; Kachkovski, A. D.; Nayyar, I. H.; Masunov, A. E.; Woodward, A. W.; Belfield, K. D. Design of a New Optical Material with Broad Spectrum Linear and Two-Photon Absorption and Solvatochromism. *J. Phys. Chem. C* **2013,** *117*, 23133–23147.

(54) Li, Y.; Ren, T.; Dong, W.-J. Tuning Photophysical Properties of Triphenylamine and Aromatic Cyano Conjugate-Based Wavelength-Shifting Compounds by Manipulating Intramolecular Charge Transfer Strength. *J. Photochem. Photobiol. A* **2013,** *251*, 1–9.

(55) Turro, N. J.; Ramamurthy, V.; Scaiano, J. C. *Modern Molecular Photochemistry of Organic Molecules*; University Science Books: California, 2010.

(56) Becke, A. D. Densityfunctional Thermochemistry. III. The Role of Exact Exchange. *J. Chem. Phys.* **1993,** *98*, 5648–5652.

(57) Yanai, T.; Tew, D. P.; Handy, N. C. A New Hybrid Exchange–Correlation Functional Using the Coulomb-Attenuating Method (Cam-B3LYP). *Chem. Phys. Lett.* **2004,** *393*, 51–57.

(58) Boese, A. D.; Martin, J. M. L. Development of Density Functionals for Thermochemical Kinetics. *J. Chem. Phys.* **2004,** *121*, 3405–3416.

(59) Mikhailov, I. A.; Bondar, M. V.; Belfield, K. D.; Masunov, A. E. Electronic Properties of a New Two-Photon Absorbing Fluorene Derivative: The Role of Hartree–Fock Exchange in the Density Functional Theory Design of Improved Nonlinear Chromophores. *J. Phys. Chem. C* **2009,** *113*, 20719–20724.

(60) Masunov, A. E. Theoretical Spectroscopy of Carbocyanine Dyes Made Accurate by Frozen Density Correction to Excitation Energies Obtained by TD-DFT. *Int. J. Quantum Chem.* **2010,** *110*, 3095–3100.

(61) Improta, R.; Barone, V.; Scalmani, G.; Frisch, M. J. A State-Specific Polarizable Continuum Model Time Dependent Density Functional Theory Method for Excited State Calculations in Solution. *J. Chem. Phys.* **2006,** *125*, 054103.

(62) Improta, R.; Scalmani, G.; Frisch, M. J.; Barone, V. Toward Effective and Reliable Fluorescence Energies in Solution by a New State Specific Polarizable Continuum Model Time Dependent Density Functional Theory Approach. *J. Chem. Phys.* **2007,** *127*, 074504.

(63) Toro, C.; Thibert, A.; De Boni, L.; Masunov, A. E.; Hernández, F. E. Fluorescence Emission of Disperse Red 1 in Solution at Room Temperature. *J. Phys. Chem. B* **2008,** *112*, 929–937.

TOC graphic

Naphthalimide dyes π-extended via thiophene